

Debye screening in strongly coupled $\mathcal{N} = 4$ supersymmetric Yang-Mills plasma

Dongsu Bak,^{1*} Andreas Karch,^{2†} and Laurence G. Yaffe^{2‡}

¹*Department of Physics, University of Seoul, Seoul 130-743, Korea*

²*Department of Physics, University of Washington, Seattle, WA 98195-1560, USA*

ABSTRACT: Using the AdS/CFT correspondence, we examine the behavior of correlators of Polyakov loops and other operators in $\mathcal{N} = 4$ supersymmetric Yang-Mills theory at non-zero temperature. The implications for Debye screening in this strongly coupled non-Abelian plasma, and comparisons with available results for thermal QCD, are discussed.

KEYWORDS: Thermal field theory, AdS/CFT correspondence.

*dsbak@mach.uos.ac.kr

†karch@phys.washington.edu

‡yaffe@phys.washington.edu

Contents

1. Introduction	1
2. Polyakov loop correlator from AdS/CFT	3
3. Correlation lengths from supergravity modes	10
4. Comparison to QCD	13
A. From weak to strong coupling	16

1. Introduction

Debye screening is a characteristic feature of any plasma. In Abelian plasmas, the electric field induced by a static test charge decreases exponentially with distance from the charge, $\langle \mathbf{E}(\mathbf{r}) \rangle \propto e^{-m_D |\mathbf{r}|}$, with m_D denoting the Debye mass (or inverse Debye screening length). The Debye mass cannot be defined so easily in a non-Abelian plasma where the field strength is only gauge-covariant, not gauge-invariant.¹ But, as discussed in Ref. [1], the Debye mass can be given a precise, non-perturbative definition (valid in both Abelian and non-Abelian theories) as the smallest inverse correlation length in symmetry channels which are odd under Euclidean time reflection. In the Hilbert space interpretation of a theory, Euclidean time reflection corresponds to the product of charge conjugation (\mathcal{C}) and time reversal (\mathcal{T}).²

In a weakly coupled plasma, the temperature T sets the scale of the energy or momentum of typical excitations (gluons or quarks in a QCD plasma). The Debye mass is parametrically smaller, $m_D \sim \sqrt{\lambda} T$, with $\lambda \equiv g^2 N_c$ the 't Hooft coupling (defined at a scale on the order of T). The Debye mass m_D may be regarded as a thermally-induced effective mass for static fluctuations in the (Euclidean) time component of the gauge field, A_0 . The equilibrium behavior on distance scales large compared to m_D^{-1} may be described by a three-dimensional effective theory which is obtained from the original four-dimensional field theory (defined on a thermal circle of circumference $\beta = 1/T$) by integrating out all non-static modes as well as the static component of A_0 . What remains are just the static, spatial components

¹For example, in the presence of a test charge $\langle \text{tr } \mathbf{E}(\mathbf{r})^2 \rangle$ is not proportional to $e^{-2m_D |\mathbf{r}|}$ at long distance. Rather, it falls exponentially as $e^{-|\mathbf{r}|/\xi}$, where ξ is the longest correlation length of the system which, in weakly coupled plasmas, is due to static magnetic fluctuations.

²This definition of the Debye mass is only applicable to theories which are invariant under \mathcal{CT} , in \mathcal{CT} invariant equilibrium states. Hence this definition cannot be used with non-zero chemical potentials. See Ref. [1] for more discussion of this point.

of the gauge field, whose dynamics are described by three-dimensional Yang-Mills theory³ with a dimensionful 't Hooft coupling $\lambda_3 = \lambda T$. In non-Abelian theories, fluctuations with wavenumbers on this scale are intrinsically non-perturbative. Three-dimensional non-Abelian Yang-Mills theories are known to develop a finite correlation length equal to the inverse of this scale times a (non-perturbative) pure number. Consequently, the mass gap m_{gap} , defined as the inverse of the longest correlation length, of a weakly coupled non-Abelian plasma is of order λT , and is parametrically smaller than the $O(\sqrt{\lambda T})$ Debye mass.

The leading weak coupling behavior of the Debye mass may be calculated from one-loop thermal perturbation theory. Subleading contributions to the Debye mass, and the leading behavior of the mass gap, depend on non-perturbative λT scale physics. In this weak coupling regime, inverse correlation lengths in different \mathcal{CT} (or Euclidean time reflection) odd symmetry channels differ only by non-perturbative $O(\lambda T)$ amounts. It is merely a convention to regard the Debye mass as the smallest inverse correlation length in all \mathcal{CT} -odd channels instead of using the correlation length in a specific symmetry channel (such as, for example, that of the imaginary part of the Polyakov loop). As explained in Ref. [1], regarding the smallest \mathcal{CT} -odd inverse correlation length as the Debye mass leads to a particularly simple relation between the next-to-leading order contribution to m_D and the expectation value of Wilson loops in three-dimensional Yang-Mills theory.

The quark-gluon plasma (QGP) produced in heavy ion collision is, for much of its evolution, thought to be rather strongly coupled [2,3], and this has stimulated much theoretical interest in understanding the dynamics of strongly coupled plasmas. Although lattice simulations are a useful technique for extracting static equilibrium quantities, observables which are sensitive to real time evolution are not generally accessible from Euclidean lattice simulations.⁴

Gauge/string (or AdS/CFT) duality has provided new theoretical tools for studying the dynamics of strongly coupled gauge theories and, in particular, strongly coupled non-Abelian plasmas. The most accessible system is maximally supersymmetric Yang-Mills ($\mathcal{N}=4$ SYM) theory in the limit of large N_c and large 't Hooft coupling. Although this theory is manifestly not QCD, at non-zero temperature $\mathcal{N}=4$ SYM describes a non-Abelian plasma composed of gauge bosons and adjoint representation fermions and scalars which shares many qualitative similarities with hot QCD. Understanding the extent to which it is, or is not, quantitatively similar to a QCD plasma is of considerable current interest.

Several quantitative comparisons of dynamic properties of $\mathcal{N}=4$ SYM and QCD plasmas in the weakly coupled regime are now available. These include the shear viscosity [11], the heavy quark energy loss (dE/dx) [12], and the photo-emission spectrum [13]. An interesting common feature has emerged from these weak-coupling comparisons: properties of $\mathcal{N}=4$ SYM agree surprisingly well with those of QCD provided one compares the two theories not

³Up to higher dimensional irrelevant operators. Scalar fields, if present, generically receive thermally induced masses comparable to the Debye mass, and may also be integrated out.

⁴However, one can attempt to constrain suitable models of spectral functions by applying maximal entropy fitting methods to numerical data for Euclidean correlators. See, for example, Refs. [4–10].

at coinciding values of the gauge coupling, but instead compares at coinciding values of the Debye mass (or other closely related thermal scales).

One would like to understand the extent to which properties of strongly coupled $\mathcal{N}=4$ SYM plasma mimic those of a QCD plasma at temperatures of perhaps $1.5\text{--}3\ T_c$ where the QCD plasma is thought to be relatively strongly coupled. In detail, this will undoubtedly depend on what observables (or ratios of observables) are considered.

As one step in this direction, our goal in this paper is to discuss what is known about the Debye mass and related phenomena associated with screening in strongly coupled $\mathcal{N}=4$ supersymmetric Yang-Mills theory (via AdS/CFT duality) and to compare with available data from lattice QCD.

Polyakov loop (or Wilson line) correlators provide the simplest probe of screening in hot gauge theories. A number of previous papers, starting with Refs. [14,15], have used AdS/CFT duality to examine the behavior of Polyakov loop correlators in strongly coupled $\mathcal{N}=4$ SYM at non-zero temperature. Confusing physical interpretations have appeared in several papers (such as the suggestion that the connected part of the correlator drops abruptly to zero at a finite separation [16]), and none of these papers specifically address the non-perturbative definition of the Debye mass mentioned above. Therefore, we revisit the analysis of Polyakov loop (and related) correlators via AdS/CFT duality. In particular, we emphasize that the connected parts of these correlators must be non-vanishing at all separations and do have exponential long distance behavior.⁵

We summarize what is known about the resulting correlation lengths in different symmetry channels, and compare with available data for corresponding correlation lengths obtained from lattice simulations in QCD at temperatures above, but near, the confinement/deconfinement transition temperature. An appendix discusses the transition from weak to strong coupling in more detail, including partial results on the first subleading $O(\lambda^{-3/2})$ strong coupling corrections to the Debye mass.

It should be noted that some authors (for example, Ref. [18,19]) refer to “screening” when discussing the behavior of the static quark potential at non-asymptotic distances, and interpret the phrase “screening length” to mean some (loosely defined) notion of when the potential deviates significantly from its zero temperature form. This is not what we mean by screening. We will always use “Debye screening” in the conventional sense, in which a screening length characterizes the asymptotic behavior of suitable correlators.

2. Polyakov loop correlator from AdS/CFT

For large N_c and large 't Hooft coupling λ , the expectation values and correlation functions of Wilson loop operators in the $\mathcal{N}=4$ theory can be calculated using the AdS/CFT correspondence. The path integral in the five dimensional gravity description in this limit is typically

⁵A closely related discussion with similar conclusions for the case of topologically trivial Wilson loop correlators at $T=0$ can be found in Ref. [17].

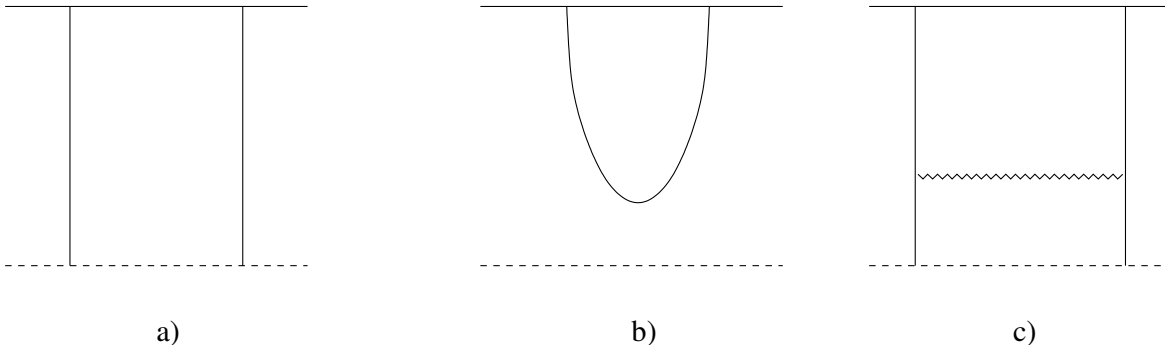


Figure 1: String configurations contributing to the Polyakov loop correlator. The upper lines represent the boundary of the geometry whereas the dashed lower lines denote the location of the black hole horizon. The periodic temporal direction is suppressed. Configuration a) depicts a disconnected worldsheet, with two independent strings running straight from the boundary to the horizon. This gives the disconnected part of the Polyakov loop correlator. Configuration b) is a smooth connected worldsheet which generates the dominant contribution to the connected correlator for sufficiently small separations. Configuration c) is a connected contribution obtained by joining two otherwise disconnected horizon-crossing string worldsheets by a small tube representing the graviton propagator. This gives the dominant contribution to the connected correlator for sufficiently large separations.

dominated by a semi-classical open string worldsheet whose boundary coincides with the loop [20, 21]. In this framework, the correlation function of two Polyakov loops,

$$C(\mathbf{x}) \equiv \langle \mathcal{P}^*(\mathbf{x}) \mathcal{P}(0) \rangle, \quad (2.1)$$

was first obtained in Refs. [14, 15]. From this, one may extract the static quark-antiquark potential (or more properly, free energy) at finite temperature in the usual fashion,

$$V_{q\bar{q}}(\mathbf{x}) \equiv -\beta^{-1} \ln C(\mathbf{x}). \quad (2.2)$$

In a non-confining phase (such as $\mathcal{N}=4$ SYM at any $T > 0$), the correlator (2.1) receives both connected and disconnected contributions. The disconnected contribution, depicted in Figure 1a, corresponds to two straight strings stretching from the boundary to the horizon. For sufficiently small separations $|\mathbf{x}|$, the connected part of the correlator is dominated by a smooth worldsheet of a string connecting the two Polyakov loops. This is illustrated in Fig. 1b. The regulated⁶ action of this worldsheet is finite and leads to a quark-antiquark free energy

⁶To regulate the infinite worldsheet area, Refs. [14, 15] subtracted the on-shell action of two straight strings stretching from the horizon to the boundary. This corresponds to renormalizing Polyakov loops in such a way that their thermal expectation value is precisely N_c . (We define the Polyakov loop $\mathcal{P}(\mathbf{x})$ as a trace of the holonomy, not the trace divided by N_c , so its expectation value in a deconfined phase is of order N_c .) Strictly speaking, this prescription is not quite right, as it corresponds to a temperature dependent renormalization condition. Temperature independent renormalization (such as holographic renormalization [22]), would produce a result for the correlator (2.1) which differs by an overall multiplicative factor. Such a finite multiplicative renormalization is irrelevant for our purposes, but its presence would complicate portions of the following discussion. Therefore, we will also adopt the simple subtraction scheme used in Ref. [14, 15].

with attractive Coulombic short distance behavior. This connected worldsheet configuration ceases to exist (as a real solution) beyond a critical separation $|\mathbf{x}| \geq r_{\text{max}} = 0.277/T$. Even before that, at a separation $r_* \equiv 0.240/T$, the regulated action of the smooth connected worldsheet (which is negative for $r < r_*$) crosses zero and becomes positive for $r_* < |\mathbf{x}| < r_{\text{max}}$.

As we discuss below, the connected Polyakov loop correlator,

$$C_{\text{conn}}(\mathbf{x}) \equiv \langle \mathcal{P}^*(\mathbf{x}) \mathcal{P}(0) \rangle - |\langle \mathcal{P} \rangle|^2, \quad (2.3)$$

must be a convex function which decreases monotonically with increasing separation. It cannot possibly drop to zero abruptly at some critical separation. Since the smooth worldsheet configuration of Fig. 1b ceases to exist when $|\mathbf{x}| > r_{\text{max}}$, there must be some other configuration which yields the dominant contribution to the connected correlator in this regime.

To identify the missing contribution, it is helpful to recall the appropriate N_c counting (as was also explained in the closely related case of correlation functions of two topologically trivial Wilson loops in Ref. [17]). The disconnected part of the correlator $C(\mathbf{x})$ scales as N_c^2 when $N_c \rightarrow \infty$. Intuitively this factor of N_c^2 can be seen in the supergravity picture by noting that the endpoints of the string at the horizon have a free Chan-Paton label indicating which D3 brane the string ends on inside the horizon. Hence there are really N_c^2 configurations of two independent strings, as depicted in Fig. 1a.⁷

Large N_c factorization implies that the disconnected part of the correlator $C(\mathbf{x})$ is the only order N_c^2 contribution; the connected part is $O(N_c^0)$, or smaller by a factor of $1/N_c^2$. Any connected worldsheet, such as the smooth connected worldsheet found in Refs. [14, 15], and sketched in Fig. 1b, does indeed produce an order one contribution to the correlator. (Hence, it makes no sense to compare the free energies of the string configurations shown in Fig. 1a and 1b, as they don't enter at the same order in N_c .)

What then is the correct string configuration which yields the leading connected contribution to the Polyakov loop correlator at large separation? The answer must be a connected worldsheet. Since, for any $|\mathbf{x}| > r_{\text{max}}$, no such configuration exists solving the equations following from the classical Nambu-Goto action, it must be a configuration with large worldsheet curvatures so that quantum fluctuations of the worldsheet become important and stabilize the configuration. When $|\mathbf{x}| \sim r_{\text{max}}$, it is difficult to find the resulting configuration explicitly. But when $|\mathbf{x}| \gg r_{\text{max}}$, the relevant worldsheet will approach a configuration of two straight strings hanging straight down toward the horizon, connected by a very thin tube, as is illustrated in Fig 1c. This corresponds to the exchange of the lightest supergravity mode coupling to both strings.

The emission and absorption vertices for supergravity modes each come with a factor of the square root of Newton's constant, $\sqrt{G_N} \sim 1/N_c$, so the connected diagram with the supergravity exchange does indeed contribute at the same N_c^0 order as does the smooth connected

⁷Equivalently, in the Euclidean description of the AdS-Schwarzschild background, where there is no horizon, each connected string worldsheet with k holes and l handles contributes at order $(N_c)^{2-k-2l}$. So the two separate worldsheets, each with a single boundary hole and no handles, in the disconnected contribution yield an overall $O(N_c^2)$ result, while a connected worldsheet with two boundary holes is $O(N_c^0)$.

worldsheet in Fig. 1b. For large separations, it is this “connected by graviton exchange” diagram that gives the leading connected contribution to the Polyakov loop correlator. The result will scale as $e^{-m|\mathbf{x}|}$, where m is the mass of the lightest supergravity mode that can be sourced by the strings.⁸

The real part of the Polyakov loop is even under \mathcal{CT} (or Euclidean time reflection), while the imaginary part is \mathcal{CT} -odd.⁹ As in the field theory discussion of Ref. [1], when considering the correlator of just the imaginary part of Polyakov loops,

$$\tilde{C}(\mathbf{x}) \equiv \langle \text{Im } \mathcal{P}(\mathbf{x}) \text{Im } \mathcal{P}(0) \rangle, \quad (2.4)$$

the symmetries of the operator $\text{Im } \mathcal{P}$ will restrict which modes can be exchanged. At large separations, the correlator $\tilde{C}(\mathbf{x})$ will be dominated by exchange of the lightest mode in the supergravity multiplet which can be sourced by the imaginary part of the Polyakov loop. Let \tilde{m} denote the mass of this mode. Which \mathcal{CT} -odd modes can contribute, and the resulting value of \tilde{m} will be discussed below. Suitably distorted Polyakov loops can couple to all symmetry channels. Therefore, what is clear on general grounds is that the Debye mass (defined as the smallest \mathcal{CT} -odd inverse correlation length) is determined by the lightest \mathcal{CT} -odd supergravity mode, while the $\text{Im } \mathcal{P}$ correlator has an exponential tail, $\tilde{C}(\mathbf{x}) \sim e^{-\tilde{m}|\mathbf{x}|}$, with a mass $\tilde{m} \geq m_D$.

To recap, the lightest mass of all supergravity modes determines the mass gap m_{gap} (or inverse of the longest correlation length) of the $\mathcal{N}=4$ SYM plasma, while it is the mass of the lightest \mathcal{CT} -odd supergravity mode which determines the Debye mass m_D . We will see shortly that the lightest supergravity mode is \mathcal{CT} even, and hence the Debye mass m_D is different (and larger) than the mass gap m_{gap} . Both of these masses will be finite in the $\lambda \rightarrow \infty$ limit, and of order T . As discussed in Ref. [1], one can also consider a more refined classification which distinguishes correlation lengths in all possible symmetry channels. In the strongly coupled $\mathcal{N}=4$ SYM plasma, these correlation lengths will be determined by the lightest masses of supergravity modes of a given symmetry. This will be discussed explicitly below.

The full Polyakov loop correlator (in the large N_c and large λ regime) is the sum of the disconnected, smooth worldsheet, and high curvature horizon-crossing worldsheet contribu-

⁸This is the same point which was made in Ref. [17], where it was argued that Wilson loop correlators at large separation are dominated by the lightest supergravity mode. There was also an early attempt [23] along these lines to identify the Debye mass for the $\mathcal{N}=4$ plasma. However, these authors considered the lightest mode in the spectrum which gives the mass gap instead of the Debye mass. In addition, at the time that paper was written the full supergravity fluctuation spectrum had not yet been worked out and it was incorrectly believed that the lightest mode would come from the dilaton. Only later was it realized that the lightest mode is actually part of the graviton.

⁹We have glossed over an irrelevant subtlety. Strictly speaking, the string configurations we have been discussing represent contributions to the correlators of Maldacena-Polyakov loops, which differ from ordinary Polyakov loops by the inclusion of a linear combination of scalar fields in the exponent [20]. However, one may choose this linear combination of scalars to be even under both \mathcal{C} and \mathcal{T} , so that the imaginary part of the loop corresponds to a \mathcal{CT} -odd operator. It should also be noted that we are assuming that one is considering the pure phase of the deconfined $SU(N_c)$ $\mathcal{N}=4$ SYM plasma in which the expectation value of the Polyakov loop is real and positive. See Ref. [1] for more discussion of the significance of this point.

tions depicted in Fig. 1,

$$C(\mathbf{x}) = C_a + C_b(\mathbf{x}) + C_c(\mathbf{x}). \quad (2.5)$$

With the renormalization prescription described in footnote 6, the disconnected contribution has a fixed value,

$$C_a = N_c^2. \quad (2.6)$$

For $|\mathbf{x}| < r_*$, the dominant connected contribution comes from the smooth worldsheet and yields

$$C_b(\mathbf{x}) = e^{-\frac{\sqrt{\lambda}}{2\pi}\mathcal{A}(|\mathbf{x}|)}, \quad (2.7)$$

where $\mathcal{A}(|\mathbf{x}|)$ is the regulated area of the smooth worldsheet configuration of Refs. [14, 15], measured in units of the AdS curvature radius. The prefactor of $\sqrt{\lambda}/(2\pi)$ is the tension of the string in AdS units. In this regime, the regulated area is negative, so the connected correlator is exponentially large compared to unity.

For $|\mathbf{x}| > r_*$, the regulated area of the smooth worldsheet is positive and its contribution is exponentially suppressed (in $\sqrt{\lambda}$). The dominant contribution to the connected correlator, in this regime, comes from the horizon-crossing string worldsheets involving thin tubes with high curvature at their ends. (A transition region whose width scales as $\lambda^{-1/2}$ connects these two regimes. This is discussed below.) For $|\mathbf{x}| \gg r_*$, this contribution to the correlator falls exponentially with increasing separation,

$$C_c(\mathbf{x}) \sim c e^{-m_{\text{gap}}|\mathbf{x}|}, \quad (2.8)$$

where m_{gap} is the lightest mass of all supergravity modes. The \mathcal{CT} -odd correlator $\tilde{C}(\mathbf{x})$ will have faster $e^{-\tilde{m}|\mathbf{x}|}$ fall-off for large separations, while for small separations $|\mathbf{x}| < r_*$ it differs from $C_{\text{conn}}(\mathbf{x})/2$ only by exponentially small (in $\sqrt{\lambda}$) contributions (arising from horizon-crossing worldsheets connected by a thin tube).

Although it is not strictly necessary for the subsequent portions of this paper, it is instructive to make a plot of the Polyakov loop correlator, and the resulting quark-antiquark potential (2.2), for various values of λ . Fig. 2 shows the connected part of the correlator for $\lambda = 10, 10^2, 10^3$ and 10^4 , while Fig. 3 shows the resulting static quark-antiquark potential, given by^{10,11}

$$V_{q\bar{q}}(\mathbf{x}) = -\beta^{-1} \ln[C_a + C_b(\mathbf{x}) + C_c(\mathbf{x})], \quad (2.9)$$

¹⁰Note that, because the static quark-antiquark potential involves the logarithm of the full correlator and not just its connected part, $V_{q\bar{q}}(\mathbf{x})$ is *not* simply proportional to the regulated area $\mathcal{A}(\mathbf{x})$ when $r < r_*$. Only when $\mathcal{A}(|\mathbf{x}|) \ll -4\pi(\ln N_c)/\sqrt{\lambda}$ does the static potential reduce to $\beta^{-1}\frac{\sqrt{\lambda}}{2\pi}\mathcal{A}(|\mathbf{x}|)$.

¹¹These plots are qualitatively, and even semi-quantitatively, correct. But they are not (and cannot be) exact for several reasons. First, only the asymptotic form (2.8) of $C_c(\mathbf{x})$ is known. As we discuss in the next section, the value of the mass gap can be extracted from known results for linearized gravitational fluctuations in the AdS-Schwarzschild background (and one finds $m_{\text{gap}} = 2.3361 \pi T$). But neither the $O(1)$ amplitude c , nor corrections to the asymptotic form, are known. To make a qualitatively correct figure, we have assumed that $C_c(\mathbf{x})$ is a pure exponential at all distances, with a value of unity at r_{max} . Second, the regulated smooth worldsheet area $\mathcal{A}(\mathbf{x})$ is only defined (as a real function) for $|\mathbf{x}| < r_{\text{max}}$. For $r_* < |\mathbf{x}| \leq r_{\text{max}}$, the contribution $C_b(\mathbf{x})$ is a nonperturbative, exponentially small correction to the correlator. Nevertheless, when plotting the

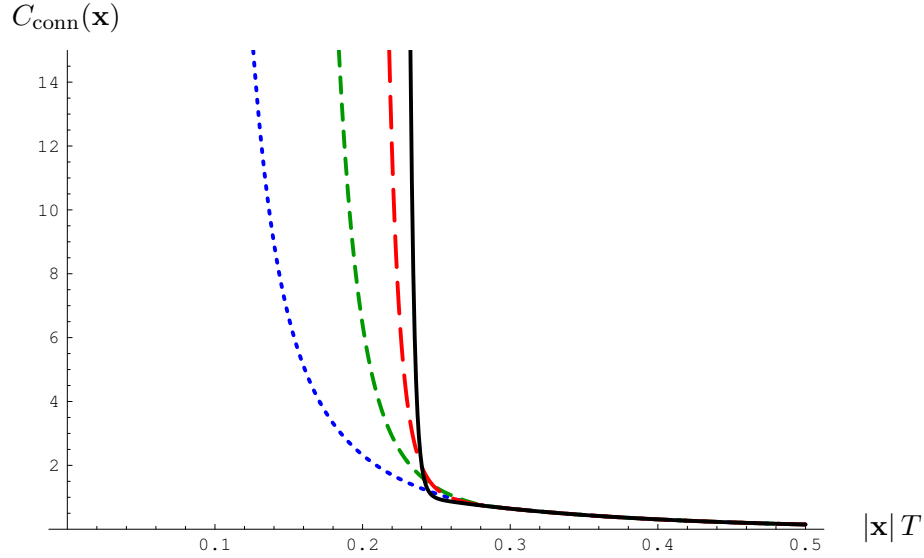


Figure 2: The connected part of the Polyakov loop correlator $C_{\text{conn}}(\mathbf{x})$ plotted as a function of the separation $|\mathbf{x}|$, for $\lambda = 10$ (blue, dotted), 10^2 (green, short dash), 10^3 (red, long dash), and 10^4 (black, solid). As $\lambda \rightarrow \infty$, the correlator develops a kink at $|\mathbf{x}| = r_* = 0.240/T$. At separations larger than r_* , the exponential decay of the correlator is nearly independent of λ .

for the same set of λ values. As these plots clearly illustrate, as λ increases the correlator, and the static potential, develop a kink at $r = r_*$, with exponential sensitivity to λ at smaller separations and almost no sensitivity to λ at larger separations.

If one considers the scaling with λ of the static quark-antiquark potential, or the force $F_{q\bar{q}}(\mathbf{x}) \equiv -\nabla V_{q\bar{q}}(\mathbf{x})$ between a static quark and antiquark, then (outside the narrow transition region) for $r < r_*$ the force is $O(\sqrt{\lambda})$ while for $r > r_*$ the force is $O(1)$. Focusing only on this comparison might lead one to think that the $r > r_*$ contribution should be regarded as a subleading $1/\lambda$ -suppressed correction to the leading large λ contribution from the smooth worldsheet. This perspective is, however, highly misleading. The smooth worldsheet (Fig. 1b) and the high-curvature horizon-crossing worldsheet (Fig. 1c) represent different stationary points of the worldsheet effective action. Except within the narrow transition region, one configuration gives the leading large λ contribution to the connected correlator $C_{\text{conn}}(\mathbf{x})$, while the other gives an exponentially suppressed relative contribution. But which configuration is leading and which is exponentially suppressed switches at the cross-over separation r_* .

correlator for any fixed finite value of λ , one must decide how to treat this contribution when $|\mathbf{x}|$ passes r_{max} . Our lack of knowledge about the right answer (which might be computable using suitable analytic continuation in the string worldsheet functional integral) amounts to a non-perturbative uncertainty which, formally, is much less important than the (unknown) corrections to the dominant contribution $C_c(\mathbf{x})$ which are suppressed by inverse powers of λ . But if one regards $C_b(\mathbf{x})$ as abruptly dropping to zero when $|\mathbf{x}|$ exceeds r_{max} then, for any finite λ , this introduces a discontinuity in the correlator (and a delta-function spike in the force $F_{q\bar{q}}(\mathbf{x}) \equiv -\nabla V_{q\bar{q}}(\mathbf{x})$) which is obviously unphysical. To avoid such spurious artifacts (and solely for the purpose of making a qualitatively correct plot), we made an ad-hoc but smooth extrapolation of $\mathcal{A}(\mathbf{x})$ beyond r_{max} . Specifically, for $|x| > r_{\text{max}}$ we used an exponential function of the form $C_b(\mathbf{x}) = \alpha + \beta e^{-\gamma|\mathbf{x}|}$ with α , β and γ determined by matching the value and first two radial derivatives of $C_b(\mathbf{x})$ at r_{max} .

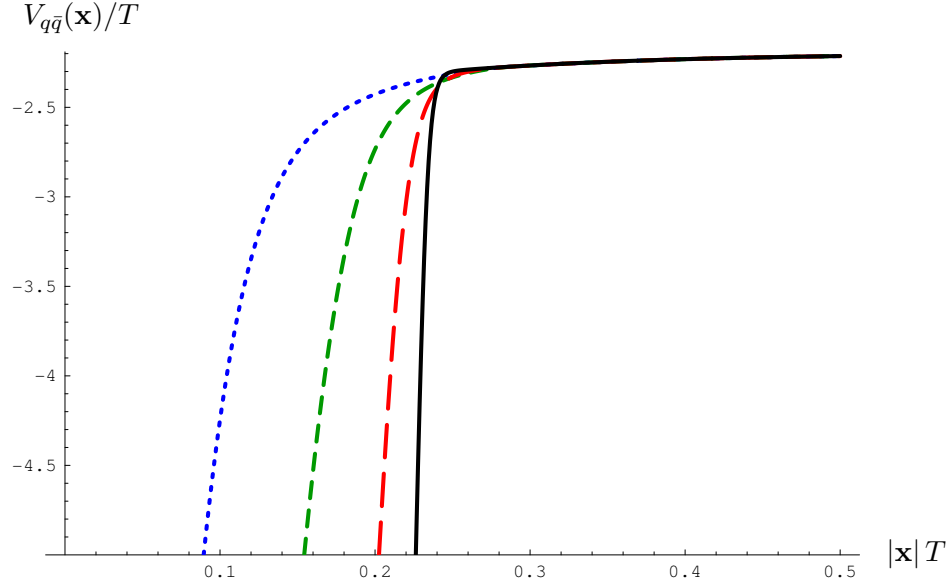


Figure 3: The static quark-antiquark potential (or free-energy) $V_{q\bar{q}}(\mathbf{x})$ plotted as a function of the separation $|\mathbf{x}|$, for $N_c = 3$ and $\lambda = 10$ (blue, dotted), 10^2 (green, short dash), 10^3 (red, long dash), and 10^4 (black, solid). As $\lambda \rightarrow \infty$, the static potential develops a kink at $|\mathbf{x}| = r_* = 0.240/T$. At separations larger than r_* , the potential continues to rise in a manner nearly independent of λ , and asymptotically approaches $-T \ln N_c^2$.

Obviously, the contribution of Fig. 1c has nothing to do with $1/\lambda$ corrections which will arise from small fluctuations around the smooth string worldsheet of Fig. 1b.

As a final point of this section, let us clarify the nature of the cross-over near r_* . In any thermal field theory, consider the Euclidean two point correlator,

$$\mathcal{G}(\mathbf{x}) = \langle W^\dagger(\mathbf{x})W(0) \rangle, \quad (2.10)$$

of any operator W , where \mathbf{x} is a spatial separation between the two operators. Finite temperature implies that one direction — which one normally regards as (Euclidean) time — is compactified. But one may equally well choose to regard the compactified direction as a spatial direction, and view the separation \mathbf{x} as defining the Euclidean time direction. A Hilbert space interpretation based on this definition of time immediately yields the spectral representation,

$$\mathcal{G}(\mathbf{x}) = \sum_n e^{-\epsilon_n |\mathbf{x}|} |c_n|^2, \quad (2.11)$$

for the correlator. Here $\{\epsilon_n\}$ are the excitation energies of eigenstates $\{|n\rangle\}$ of the Hamiltonian (for the spatially compactified system) and $c_n \equiv \langle n|W|0\rangle$. Since every term in the sum is positive, this representation shows that the correlator $\mathcal{G}(\mathbf{x})$, as a function of separation $|\mathbf{x}|$, is positive, monotonically decreasing, and convex. Moreover, if the connected part of the correlator, $\mathcal{G}(\mathbf{x}) - \mathcal{G}(\infty)$, is non-zero at some separation \mathbf{x} , then it must be non-zero (and positive) at all \mathbf{x} . In other words, a connected correlator cannot be non-zero for some range of separations, and then vanish identically beyond a critical separation.

These general principles are completely consistent with the above description of the Polyakov loop correlator $C(\mathbf{x})$. But the change in behavior near r_* implies that two very different energy scales contribute to the spectral representation for $C(\mathbf{x})$. Specifically, there are states with $O(T)$ energies starting at m_{gap} , and in addition states with $O(\sqrt{\lambda}T)$ energies starting at a threshold of $\eta\sqrt{\lambda}/(2\pi)$, where $\eta = 20.7T$ is the slope with which the regulated area of the smooth worldsheet crosses zero at $|\mathbf{x}| = r_*$, $\mathcal{A}(|\mathbf{x}|) \sim \eta(|\mathbf{x}| - r_*)$. For any finite value of the 't Hooft coupling λ , the correlator will be a smooth convex function of separation. The low energy states completely dominate when $|\mathbf{x}|$ is big compared to r_* while the high energy states dominate for $|\mathbf{x}|$ well below r_* . High and low energy states make comparable contributions only in a narrow cross-over region around r_* , whose relative width $\delta r/r_*$ scales as $\lambda^{-1/2}$. In the $\lambda \rightarrow \infty$ limit, this width shrinks to zero and the correlator develops a kink, but remains positive, monotonic, and convex.

3. Correlation lengths from supergravity modes

Fortunately the analysis of the complete IIB supergravity spectrum, in R -symmetry singlet channels, on the AdS black hole background has already been performed in Ref. [24] (following earlier work on portions of the spectrum in Ref. [25]). In those papers the spectrum was presented as glueball masses of a three-dimensional confining gauge theory (containing Kaluza-Klein towers whose spacing is comparable to the mass of the lightest glueballs). We find it much more natural to interpret the supergravity spectrum as giving us information about the finite temperature $\mathcal{N}=4$ SYM plasma. As just discussed, the supergravity spectrum directly yields the spatial correlation lengths, in different symmetry channels, of the hot plasma.

For the reader's convenience, we reproduce in Table 1 the results for the supergravity modes from Ref. [24]. The relevant supergravity fields are the metric $G_{\mu\nu}$, the dilaton-axion pair $e^{-\phi} + ia$, and the NSNS and RR two forms $B_{\mu\nu}$ and $C_{\mu\nu}$. For each one of these fields, the mass¹² of the lightest mode with a given polarization is listed, in units of πT , together with its transformation properties J^{PCT} under (3+1)-dimensional Poincaré symmetry. In this table (as in Ref. [24]), the longitudinal direction defined by the spatial wave vector \mathbf{k} of the mode is taken to point in the x_3 direction. For our application to two-point correlators, this corresponds to the direction of the spatial separation \mathbf{x} of the operators. The indices i and j denote transverse spatial directions (corresponding to x_1 and x_2), and a refers to the directions along the internal S^5 . The table also lists the quantum numbers $\mathcal{J}_{R_y}^{CR_t}$ for the $O(2) \times Z_2$ Euclidean symmetry in the x, y, t plane transverse to the longitudinal direction, plus charge conjugation, which is the relevant symmetry group for a transfer matrix in the x_3 direction. Here, \mathcal{J} is the two-dimensional angular momentum, R_t is the eigenvalue corre-

¹²This terminology is a bit sloppy. The mass m_0 is the smallest magnitude of an imaginary wavevector $\vec{\kappa}$ for which the linearized supergravity equations for the various fields (in the Euclidean AdS black hole geometry) admit solutions whose only spacetime dependence is of the form $\exp(\vec{\kappa} \cdot \mathbf{x})f(u)$, where u is the radial AdS coordinate. This is precisely what is needed to determine the correlation lengths of Euclidean correlators.

SUGRA mode	J^{PCT}	$\mathcal{J}_{R_y}^{CR_t}$	m_0	SYM operator
G_{00}	0^{+++}	0_+^{++}	2.3361	T_{00}
G_{ij}	2^{+++}	2^{++}	3.4041	T_{ij}
a	0^{-+-}	0_-^{+-}	3.4041	$\text{tr } E \cdot B$
ϕ	0^{+++}	0_+^{++}	3.4041	\mathcal{L}
G_{i0}	1^{++-}	1^{+-}	4.3217	T_{i0}
B_{ij}	1^{+--}	0_-^{+-}	5.1085	\mathcal{O}_{ij}
C_{ij}	1^{--+}	0_+^{+-}	5.1085	\mathcal{O}_{30}
B_{i0}	1^{--+}	1^{--}	6.6537	\mathcal{O}_{i0}
C_{i0}	1^{+--}	1^{-+}	6.6537	\mathcal{O}_{3j}
G_a^a	0^{+++}	0_+^{++}	7.4116	$\text{tr } F^4$

Table 1: Spectrum of R -singlet IIB supergravity modes in units of πT , together with SYM operators dual to the indicated mode (see text for details). J^{PCT} are quantum numbers for (3+1)-dimensional Poincaré symmetry, while $\mathcal{J}_{R_y}^{CR_t}$ are quantum numbers for the $O(2) \times Z_2$ Euclidean symmetry in the xyt -plane transverse to the x_3 direction (plus charge conjugation).

sponding to the reflection $t \rightarrow -t$, R_y is the eigenvalue for the reflection $y \rightarrow -y$, and C , as usual, is the eigenvalue for charge conjugation. (Note that only one-dimensional irreducible representations with $\mathcal{J} = 0$ need to be labeled with R_y . Two dimensional representations with $\mathcal{J} \neq 0$ contain components with both signs of R_y .) As mentioned in the Introduction, Euclidean time reflection is the product of time reversal and charge conjugation, so $R_t = CT$.

The field $B_{\mu\nu}$ couples to the current $J_F^{\mu\nu}$ of the fundamental string which is electrically charged, while the $C_{\mu\nu}$ field couples to the magnetically charged D-string current. Hence these fields are both charge conjugation odd, but have opposite parity and time reversal assignments.

Using the standard dictionary of the AdS/CFT correspondence, all operators dual to the above supergravity modes can be identified. In particular, the operator dual to the graviton corresponds to the energy-momentum tensor $T_{\mu\nu}$ of $\mathcal{N}=4$ super Yang-Mills theory.¹³ The axion is dual to the Pontryagin density $\frac{1}{4} \text{tr } F^{\mu\nu} \tilde{F}_{\mu\nu} = \text{tr } E \cdot B$, whereas the dilaton is dual to the $\mathcal{N}=4$ Lagrange density $\mathcal{L} = \frac{1}{4} \text{tr } F^{\mu\nu} F_{\mu\nu} + \dots$. Since the \mathcal{C} and \mathcal{T} quantum numbers of E and B are $-+$ and $--$, respectively, one finds $+-$ for $E \cdot B$, and $++$ for \mathcal{L} , in agreement with the listed assignments for the axion and dilaton modes. The operator dual to the lowest mode of G_a^a involves the trace of four powers of the field strength; a more explicit form may

¹³The analysis of Ref. [24] used a gauge choice in which the independent modes of the metric and two-form fluctuations correspond to polarizations without any indices in the longitudinal (x_3) or AdS radial directions. Hence the absence of these field components in the table. Because $T_{\mu\nu}$ is conserved, the corresponding “missing” components of the energy-momentum tensor (T_{03} , T_{i3} and T_{33}) are not independent from the components shown in the table.

be found in Ref. [26]. The two-form fields $B_{\mu\nu}$ and $C_{\mu\nu}$ couple to the SYM antisymmetric tensor operator $\mathcal{O}_{\mu\nu}$ [27], which is the $\mathcal{N}=4$ completion of the QCD operator

$$O_{\mu\nu} \equiv \text{tr} \left[F_{\mu\alpha} F^{\alpha\beta} F_{\nu\beta} + \frac{1}{4} F_{\mu\nu} F^{\alpha\beta} F_{\alpha\beta} \right]. \quad (3.1)$$

Five dimensional antisymmetric tensor fields have in general six real independent on-shell degrees of freedom. But in type IIB supergravity on $\text{AdS}_5 \times S^5$, there is an extra constraint linearly relating $B_{\mu\nu}$ and $C_{\mu\nu}$ [24]. Hence the total on-shell degrees of freedom in these two fields are reduced to only six. Among these, B_{ij} is dual to \mathcal{O}_{ij} and C_{ij} to $\epsilon_{ij03} \mathcal{O}_{03}$. One can also find that B_{i0} is dual to \mathcal{O}_{i0} while C_{i0} is dual to $\epsilon_{i03j} \mathcal{O}_{3j}$. Since $B_{\mu\nu} + iC_{\mu\nu}$ or $e^{-\phi} + ia$ are multiplets of the $SL(2, R)$ symmetry of the tree-level IIB supergravity, their spectrum should be degenerate. Indeed this can be checked from Table 1. Note that the different correlation lengths for \mathcal{O}_{12} and \mathcal{O}_{3j} reflect our choice of x_3 as the longitudinal direction.

Examining Table 1, one sees that the true mass gap of the $\mathcal{N}=4$ SYM plasma (in the $\lambda \rightarrow \infty$ and $N_c \rightarrow \infty$ limits) arises from the time-time component of the graviton. This belongs to the \mathcal{CT} even sector, as asserted earlier. The SYM mass gap is thus

$$m_{\text{gap}} = 2.3361 (\pi T), \quad (3.2)$$

and this characterizes the longest correlations in this non-Abelian plasma. On the other hand, the lowest mass in a \mathcal{CT} -odd channel comes from the response of the axion field a . Therefore the Debye mass for the $\mathcal{N}=4$ SYM plasma in the strong coupling limit is given by

$$m_D = 3.4041 (\pi T). \quad (3.3)$$

The imaginary part of the Polyakov loop has $J^{PCT} = 0^{++}$ or $\mathcal{J}_{R_y}^{CR_t} = 0_+^{--}$ and, in particular, is \mathcal{C} -odd. Hence exchange of the \mathcal{C} -even (but \mathcal{T} -odd) axion field cannot contribute to the $\text{Im } \mathcal{P}$ correlator. Moreover, as Table 1 shows, there is no supergravity field with 0^{++} quantum numbers. However, the three-form field strength $(dC)_{123}$ does have precisely this symmetry, and its spectrum is the same as that of C_{12} for our choice of longitudinal direction x_3 . Consequently, exchange of the two-form C can contribute to the $\text{Im } \mathcal{P}$ correlator, implying that¹⁴

$$\tilde{m} = 5.1085 (\pi T). \quad (3.4)$$

Note that the supergravity analysis predicts not only the values of various correlation lengths, it also identifies which local operators in the dual field theory couple most directly to the lightest modes (in the strong coupling regime). In principle, it should be possible to confirm the predictions (3.2)–(3.4) via lattice simulations of the relevant correlators in $\mathcal{N}=4$ SYM — but this is not yet practically feasible.

¹⁴An open string does not source the two-form C at tree level, but fermion fluctuations on the string do couple to the RR field-strength. This implies that the $e^{-\tilde{m}|\mathbf{x}|}$ tail in the $\tilde{C}(\mathbf{x})$ correlator will have a coefficient suppressed by $1/\lambda$ relative to the short distance contributions. This shifts the center of the cross-over region by a tiny relative amount of order $O[(\ln \lambda)/\lambda]$.

4. Comparison to QCD

Data for screening masses (*i.e.*, inverse correlation lengths) in various symmetry channels, in $SU(2)$ and $SU(3)$ pure gauge theory, are available from $4d$ lattice simulations [28–31], as well as $3d$ simulations using the dimensionally reduced high temperature effective theory [32–36]. Results from both approaches are generally consistent with each other at the 10–15% level down to $T = 2T_c$. (For a good summary of the status of lattice calculations of thermal correlation lengths, see Ref. [37].) The dimensional reduction approach allows one to treat (with no additional computational complexity) QCD with any number of massless fermions. Using this approach, Ref. [32] reports results for many different symmetry channels and zero, two, three or four quark flavors.

In Yang-Mills theory, the ratios of screening masses to the temperature are very nearly temperature independent for $1.5T_c \leq T \lesssim 4T$, but (at least in the 0^{+++} and 0^{+-+} channels) decrease substantially as the temperature drops below $1.5T_c$ and approaches the confinement transition [28, 29]. The degree of similarity between thermal QCD and $\mathcal{N}=4$ SYM is surely greatest within the window, $1.5T_c \leq T \lesssim 4T$, where screening masses scale linearly with temperature. Comparison of results for screening masses in $SU(2)$ and $SU(3)$ Yang-Mills theory reveal very little dependence on N_c if $\lambda = g^2 N_c$ is held fixed. Consequently, the difference between $N_c = 3$ and $N_c = \infty$ is expected to be quite small [32].

To make specific comparisons, we will use the results from Ref. [32] for $T = 2T_c$,¹⁵ and we will also focus on the case of $N_f = 2$, where simulations were performed at a finer lattice spacing than for other (non-zero) values of N_f . QCD lattice simulations find that the smallest thermal screening mass is in the scalar 0^{+++} channel, in agreement with the strong coupling $\mathcal{N}=4$ SYM analysis. Table 2 shows results from Ref. [32] for the ratios of screening masses in different symmetry channels relative to the mass gap (the lightest screening mass) for $N_f = 2$ QCD at $T = 2T_c$, together with the corresponding $\lambda = \infty$ $\mathcal{N}=4$ SYM results from Table 1.¹⁶ The same information is displayed graphically in Fig. 4.

The lightest \mathcal{CT} (or R_t) odd screening mass, which defines the Debye mass, is in the $\mathcal{J}_{R_y}^{CR_t} = 0_-^{+-}$ (axion) channel in both QCD and strongly coupled $\mathcal{N}=4$ SYM. As show in the above table and figure, there is essentially perfect agreement between the two theories for the value of the Debye mass to mass gap ratio, $m_D/m_{\text{gap}} \approx 1.46$. This remarkable agreement (to better than a percent) is surely somewhat fortuitous; in other channels the discrepancy between QCD and $\mathcal{N}=4$ SYM for these screening mass to mass gap ratios varies between a few percent and 30% (for the 2^{++} channel). Overall, however, there is rather good agreement between the two theories.

¹⁵Actually, these results are for $T = 2\Lambda_{\overline{MS}}$. The ratio of $T_c/\Lambda_{\overline{MS}}$ is close to one, but is not known with very high accuracy when $N_f \neq 0$.

¹⁶In contrast to the (lighter) spin 0 and spin 2 channels, Ref. [32] specified the time reflection symmetry but not the charge conjugation properties of the spin one operators they used. We have assumed that their spin one results should be compared with the lightest $\mathcal{J} = 1$ channels with the given value of R_t which, for strongly coupled $\mathcal{N}=4$ SYM, are the spin one channels indicated in Table 2 and Fig. 4.

$\mathcal{J}_{R_y}^{CR_t}$	$N_f = 2$ QCD	$\mathcal{N} = 4$ SYM	SUGRA mode
0_-^{+-}	1.45(4)	1.46	a
0_+^{--}	1.79(4)	2.19	C_{ij}
2^{++}	2.05(6)	1.46	G_{ij}
0_-^{-+}	2.12(7)	2.19	B_{ij}
1^{+-}	2.31(10)	1.85	G_{i0}
1^{-+}	2.79(12)	2.85	C_{i0}

Table 2: Ratios of screening masses in indicated symmetry channels to the mass gap, for $N_f = 2$ QCD at $2T_c$, and $\lambda = \infty, N_c = \infty$ $\mathcal{N} = 4$ SYM. For both QCD and strongly coupled $\mathcal{N} = 4$ SYM, the mass gap is the screening mass in the 0_+^{++} channel.

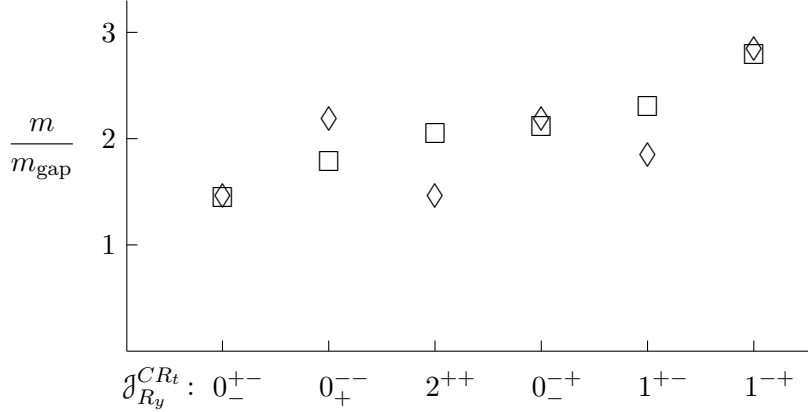


Figure 4: Ratios of screening masses in indicated symmetry channels to the mass gap (the 0_+^{++} screening mass), for $N_f = 2$ QCD at $2T_c$ (squares), and $\lambda = \infty$ $\mathcal{N} = 4$ SYM (diamonds). The reported statistical errors on the QCD lattice results are smaller than size of the squares.

Instead of focusing on ratios of screening masses, if one looks at their absolute size (in units of the temperature), then one finds that screening masses in QCD (at $T \approx 2T_c$) [32] are significantly smaller than in $\lambda = \infty$ $\mathcal{N} = 4$ SYM:

$$\frac{m_{\text{gap}}}{\pi T} = \begin{cases} 1.25(2), & N_f = 2 \text{ QCD}, T = 2T_c; \\ 2.34, & \mathcal{N} = 4 \text{ SYM}, \lambda = \infty, \end{cases} \quad (4.1)$$

$$\frac{m_D}{\pi T} = \begin{cases} 1.80(4), & N_f = 2 \text{ QCD}, T = 2T_c; \\ 3.40, & \mathcal{N} = 4 \text{ SYM}, \lambda = \infty. \end{cases} \quad (4.2)$$

In $\mathcal{N} = 4$ SYM, these masses (divided by T) are dimensionless functions depending only

on the coupling λ . In the weak coupling regime, m_{gap}/T vanishes linearly as $\lambda \rightarrow 0$, while m_{D}/T scales as $\sqrt{\lambda}$. Presumably, both masses grow monotonically with increasing λ and asymptote to the above $\lambda = \infty$, $\mathcal{N} = 4$ SYM values.

The smaller values for the Debye mass (and the mass gap) in QCD at $2T_c$, as compared to $\lambda = \infty$ SYM values, naturally suggests that QCD plasma, in this temperature range, is most similar to $\mathcal{N} = 4$ SYM plasma at an intermediate value of λ which is neither in the asymptotically weak, nor asymptotically strong coupling regimes. To test this hypothesis quantitatively, it will be necessary to compute subleading (in $1/\lambda$) corrections to $\lambda = \infty$ screening masses in $\mathcal{N} = 4$ SYM plasma. The Appendix discusses this in more detail, and reports some partial results on the first subleading correction to m_{D} .

Other possible extensions of this work include a comparison of correlation lengths associated with flavor current correlators probing the dynamics of fundamental representation matter added to $\mathcal{N} = 4$ SYM. In the gravitational dual, this corresponds to the addition of D7 flavor branes as described in Ref. [38]. Lattice data is now available for a variety of mesonic correlation lengths in hot QCD [8, 37, 39, 40]. We hope that this, and similar work, will clarify the degree to which $\mathcal{N} = 4$ supersymmetric Yang-Mills plasma can mimic quantitative properties of the quark-gluon plasma produced in heavy ion collisions.

Acknowledgments

D.B. would like to thank the Particle Theory Group of the University of Washington for the warm hospitality. L.G.Y thanks the Galileo Galilei Institute for Theoretical Physics for its hospitality, and the INFN for partial support during the completion of this work. We also thank Ofer Aharony and Michael Gutperle for helpful conversations and communications. This work was supported in part by the U.S. Department of Energy under Grant No. DE-FG02-96ER40956 and by KOSEF SRC CQeST R11-2005-021.

A. From weak to strong coupling

The leading weak-coupling behavior of the Debye mass in $\mathcal{N}=4$ SYM is determined by the one-loop thermal correction to the gluon self-energy. One easily finds the lowest-order result [41, 42]

$$m_{\text{D}}^{(0)} = \sqrt{2\lambda} T. \quad (\text{A.1})$$

This is larger than the corresponding result for massless QCD (with $N_c = 3$) by a factor of $\sqrt{6} \approx 2.45$ for $N_f = 0$, $3/\sqrt{2} \approx 2.12$ for $N_f = 2$, or 2 for $N_f = 3$ (with N_f the number of quark flavors).

The next-to-leading order weak-coupling correction to m_{D} contains a logarithmic term whose coefficient may be easily extracted using perturbative effective field theory methods, together with a non-perturbative $O(\lambda T)$ contribution which can only be computed via numerical lattice simulations. The analysis of Ref. [1] shows that changing the matter content of the theory from QCD to that of $\mathcal{N}=4$ SYM does not affect the next-to-leading order correction to the Debye mass (other than changing the value of $m_{\text{D}}^{(0)}$). The result is

$$m_{\text{D}} = m_{\text{D}}^{(0)} + \frac{\lambda T}{4\pi} \ln \frac{m_{\text{D}}^{(0)}}{\lambda T} + \kappa \lambda T + O(\lambda^{3/2} T), \quad (\text{A.2})$$

with the non-perturbative coefficient $\kappa = 0.64(2)$ for $N_c = 3$ [35].¹⁷ The weak-coupling expansion of the Debye mass is much better behaved in $\mathcal{N}=4$ SYM than in QCD due to the larger value of $m_{\text{D}}^{(0)}$. (The $O(\lambda T)$ terms only become larger than $m_{\text{D}}^{(0)}$ when λ exceeds 5.6.)

The strong-coupling results for inverse correlation lengths derived in this paper have corrections which are suppressed by inverse powers of the 't Hooft coupling λ , arising from α' corrections to type IIB supergravity. The first subleading corrections for the dilaton were investigated in Ref. [25], with the result

$$m_{\phi} = 3.4041 [1 - 1.39 \zeta(3) \lambda^{-3/2} + \dots] (\pi T). \quad (\text{A.3})$$

To find the analogous subleading correction for the Debye mass, one cannot invoke the $SL(2, R)$ symmetry of the tree-level IIB supergravity; an independent calculation of the axion mode is required. Corrections to the axion mass come from the original IIB action expanded around the α' corrected black hole background, as well as from new eight-derivative terms in the action affecting quadratic fluctuations around the original black hole background. Unfortunately these latter terms are not completely known at present. In principle these terms should follow by supersymmetry from the well known R^4 corrections, but the details are not yet fully understood.

Possible corrections to the Debye mass arise from terms quadratic in the axion coupled to either the background curvature or the 5-form field strength. Ref. [43] has an explicit

¹⁷For $SU(2)$, $\kappa = 0.63(2)$ [35]. Determinations of κ from lattice simulations with $N_c > 3$ have, to our knowledge, not yet been performed, but the dependence of κ on N_c is clearly very weak. Comparisons with four-dimensional simulations also show that, in pure Yang-Mills, $O(\lambda^{3/2} T)$ and higher contributions are not large compared to the $O(\lambda T)$ terms when $T \gtrsim 2T_c$ [35].

proposal for all the terms involving the axion and the curvature. The axion appears in the non-perturbative contributions to the modular functions f_k , but all those contributions are due to D-instantons and are exponentially suppressed by $e^{-1/g_s} \sim e^{-4\pi N_c/\lambda}$. They are thus irrelevant in the large N_c limit. The other two terms that are potentially important are $12f_0 R^2 DPDP$ and $6f_2 R^2 (DPDP + D\bar{P}D\bar{P})$, where P is proportional to the first derivative of the axion-dilaton pair. The axion derivative is the imaginary part of P . The factors f_0 and f_2 are different functions of the axion-dilaton pair, but their leading weak coupling (*i.e.*, large N_c) behavior is identical. In this limit, the axion contribution miraculously cancels between the above two terms from the proposal of Ref. [43]. Unfortunately the action proposed by Ref. [43] is not the unique $SL(2, R)$ invariant extension of the known terms involving NSNS sector fields. In the absence of any rigorous arguments, an explicit calculation of the coefficient of the $R^2(\partial^2 a)^2$ term from a tree level 4-point function is needed. This computation has been performed recently in Ref. [44] with the result that the coefficient is non-zero, in contradiction with the proposal of Ref. [43]. However the precise normalization has not been determined, so a complete calculation of the sub-leading correction to the Debye mass is not possible at this time. In addition there will be non-vanishing terms involving the 5-form field strength, which is non-zero in the AdS black-hole background, and its derivatives. While some of these terms are known, see Ref. [45, 46], there may be additional unknown terms involving the coupling of the 5-form field strength to the axion.

We have, nevertheless, calculated the $\lambda^{-3/2}$ corrections that would follow from the simple conjecture of Ref. [43]. In that case the axion fluctuation satisfies the equation of motion

$$\partial_m \sqrt{-g} g^{mn} e^{2\phi} \partial_n a = 0, \quad (\text{A.4})$$

where one has to use the α' corrected dilaton profile and metric in the $10d$ Einstein frame. Using the same shooting method as in Ref. [25], we find that the next-to-leading order (NLO) result for the Debye mass is

$$m_D = 3.4041 \left[1 - 0.52 \zeta(3) \lambda^{-3/2} + \dots \right] (\pi T). \quad (\text{A.5})$$

As with the dilaton, this correction leads to a smaller Debye mass as λ decreases. Neglecting all further higher order corrections, this result becomes negative at $\lambda = 0.731$.

If one assumes, for the sake of discussion, that the additional $\lambda^{-3/2}$ corrections due to eight-derivative terms in the corrected IIB action do not significantly change the result (A.5), then it is interesting to compare the strong and weak coupling expressions for the Debye mass. Figure 5 shows this comparison, along with one possible smooth interpolation between weak and strong coupling obtained by adding next-to-next-to-leading order (NNLO) terms to both Eq. (A.2) and Eq. (A.5) and adjusting their coefficients to make the resulting curves tangent at a single point.¹⁸

¹⁸Specifically, $0.6 \lambda^{3/2} T$ was added to the weak coupling result (A.2), and $-5.0 \lambda^{-3}$ added inside the bracket of the strong coupling result (A.5). The resulting weak and strong coupling curves are tangent at $\lambda = 3.0$.

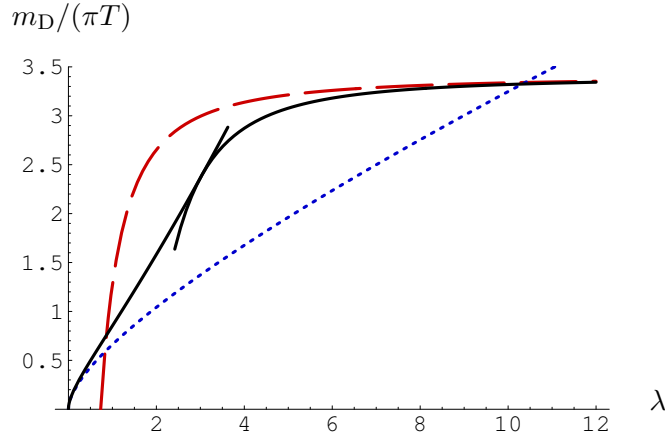


Figure 5: Debye mass in $\mathcal{N}=4$ SYM as a function of λ . The dashed (red) curve shows the NLO strong-coupling result (A.5) based on the conjecture of Ref. [43] while the dotted (blue) curve shows the NLO weak-coupling result (A.2). The solid (black) curve lying between these two NLO curves (for intermediate couplings) shows a smooth interpolation obtained by adding NNLO terms to both expansions, as explained in footnote 18, and adjusting their coefficients to produce results which are tangent at a single point.

This choice of interpolation is certainly not unique, but it illustrates a reasonable choice given the available asymptotic information. This particular interpolation suggests that an $\mathcal{N}=4$ SYM plasma will have a Debye mass which coincides with the $T = 2T_c$ QCD result (4.2) when $\lambda_{\text{SYM}} \approx 2.5$. The strong and weak coupling results would match better (*i.e.*, smaller NNLO terms would be needed to make them interpolate smoothly) if the unknown additional contributions to the Debye mass from $R^2(\partial^2 a)^2$ terms in the effective action lead to a larger (more negative) correction at order $\lambda^{-3/2}$.

References

- [1] P. Arnold and L. G. Yaffe, *The non-Abelian Debye screening length beyond leading order*, *Phys. Rev.* **D52** (1995) 7208–7219, [[hep-ph/9508280](#)].
- [2] E. V. Shuryak, *What RHIC experiments and theory tell us about properties of quark-gluon plasma?*, *Nucl. Phys.* **A750** (2005) 64–83, [[hep-ph/0405066](#)].
- [3] M. J. Tannenbaum, *Recent results in relativistic heavy ion collisions: From ‘a new state of matter’ to ‘the perfect fluid’*, *Rept. Prog. Phys.* **69** (2006) 2005–2060, [[nucl-ex/0603003](#)].
- [4] M. Asakawa, T. Hatsuda, and Y. Nakahara, *Maximum entropy analysis of the spectral functions in lattice QCD*, *Prog. Part. Nucl. Phys.* **46** (2001) 459–508, [[hep-lat/0011040](#)].
- [5] Y. Nakahara, M. Asakawa, and T. Hatsuda, *Hadronic spectral functions in lattice QCD*, *Phys. Rev.* **D60** (1999) 091503, [[hep-lat/9905034](#)].
- [6] G. Aarts, S. Hands, S.-y. Kim, and J. M. Martinez Resco, *On meson spectral functions at high temperature and nonzero momentum*, *PoS LAT2005* (2006) 182, [[hep-lat/0509062](#)].
- [7] G. Aarts and J. M. Martinez Resco, *Continuum and lattice meson spectral functions at nonzero momentum and high temperature*, *Nucl. Phys.* **B726** (2005) 93–108, [[hep-lat/0507004](#)].
- [8] S. Wissel, E. Laermann, S. Shcheredin, S. Datta, and F. Karsch, *Meson correlation functions at high temperatures*, *PoS LAT2005* (2006) 164, [[hep-lat/0510031](#)].
- [9] S. Datta, F. Karsch, P. Petreczky, and I. Wetzorke, *Meson correlators above deconfinement*, *J. Phys.* **G31** (2005) S351–S356, [[hep-lat/0412037](#)].
- [10] H. B. Meyer, *A calculation of the shear viscosity in $SU(3)$ gluodynamics*, [arXiv:0704.1801](#) [[hep-lat](#)].
- [11] S. C. Huot, S. Jeon, and G. D. Moore, *Shear viscosity in weakly coupled $\mathcal{N}=4$ super Yang-Mills theory compared to QCD*, [hep-ph/0608062](#).
- [12] P. M. Chesler and A. Vuorinen, *Heavy flavor diffusion in weakly coupled $\mathcal{N}=4$ super Yang-Mills theory*, *JHEP* **11** (2006) 037, [[hep-ph/0607148](#)].
- [13] S. Caron-Huot, P. Kovtun, G. D. Moore, A. Starinets, and L. G. Yaffe, *Photon and dilepton production in supersymmetric Yang-Mills plasma*, *JHEP* **12** (2006) 015, [[hep-th/0607237](#)].
- [14] S.-J. Rey, S. Theisen, and J.-T. Yee, *Wilson-Polyakov loop at finite temperature in large N gauge theory and anti-de Sitter supergravity*, *Nucl. Phys.* **B527** (1998) 171–186, [[hep-th/9803135](#)].
- [15] A. Brandhuber, N. Itzhaki, J. Sonnenschein, and S. Yankielowicz, *Wilson loops in the large N limit at finite temperature*, *Phys. Lett.* **B434** (1998) 36–40, [[hep-th/9803137](#)].
- [16] S. S. Gubser, *Comparing the drag force on heavy quarks in $\mathcal{N}=4$ super-Yang-Mills theory and QCD*, [hep-th/0611272](#).
- [17] D. J. Gross and H. Ooguri, *Aspects of large N gauge theory dynamics as seen by string theory*, *Phys. Rev.* **D58** (1998) 106002, [[hep-th/9805129](#)].
- [18] O. Kaczmarek and F. Zantow, *The screening length in hot QCD*, *PoS LAT2005* (2006) 177, [[hep-lat/0510093](#)].

- [19] H. Liu, K. Rajagopal, and U. A. Wiedemann, *An AdS/CFT calculation of screening in a hot wind*, [hep-ph/0607062](#).
- [20] J. M. Maldacena, *Wilson loops in large N field theories*, *Phys. Rev. Lett.* **80** (1998) 4859–4862, [[hep-th/9803002](#)].
- [21] S.-J. Rey and J.-T. Yee, *Macroscopic strings as heavy quarks in large N gauge theory and anti-de Sitter supergravity*, *Eur. Phys. J.* **C22** (2001) 379–394, [[hep-th/9803001](#)].
- [22] C. R. Graham and E. Witten, *Conformal anomaly of submanifold observables in AdS/CFT correspondence*, *Nucl. Phys.* **B546** (1999) 52–64, [[hep-th/9901021](#)].
- [23] U. H. Danielsson, E. Keski-Vakkuri, and M. Kruczenski, *Spherically collapsing matter in AdS, holography, and shellons*, *Nucl. Phys.* **B563** (1999) 279–292, [[hep-th/9905227](#)].
- [24] R. C. Brower, S. D. Mathur, and C.-I. Tan, *Glueball spectrum for QCD from AdS supergravity duality*, *Nucl. Phys.* **B587** (2000) 249–276, [[hep-th/0003115](#)].
- [25] C. Csaki, H. Ooguri, Y. Oz, and J. Terning, *Glueball mass spectrum from supergravity*, *JHEP* **01** (1999) 017, [[hep-th/9806021](#)].
- [26] E. D’Hoker and D. Z. Freedman, *Supersymmetric gauge theories and the AdS/CFT correspondence*, [hep-th/0201253](#).
- [27] S. R. Das and S. P. Trivedi, *Three brane action and the correspondence between $\mathcal{N}=4$ Yang Mills theory and anti de Sitter space*, *Phys. Lett.* **B445** (1998) 142–149, [[hep-th/9804149](#)].
- [28] S. Datta and S. Gupta, *Does the QCD plasma contain propagating gluons?*, *Phys. Rev.* **D67** (2003) 054503, [[hep-lat/0208001](#)].
- [29] S. Datta and S. Gupta, *Screening masses in $SU(2)$ pure gauge theory*, *Phys. Lett.* **B471** (2000) 382–387, [[hep-lat/9906023](#)].
- [30] S. Datta and S. Gupta, *Dimensional reduction and screening masses in pure gauge theories at finite temperature*, *Nucl. Phys.* **B534** (1998) 392–416, [[hep-lat/9806034](#)].
- [31] S. Datta and S. Gupta, *Dimensional reduction in high temperature gauge theories*, [hep-ph/9809382](#).
- [32] A. Hart, M. Laine, and O. Philipsen, *Static correlation lengths in QCD at high temperatures and finite densities*, *Nucl. Phys.* **B586** (2000) 443–474, [[hep-ph/0004060](#)].
- [33] O. Philipsen, *Debye screening in the QCD plasma*, [hep-ph/0010327](#).
- [34] A. Hart and O. Philipsen, *The spectrum of the three-dimensional adjoint Higgs model and hot $SU(2)$ gauge theory*, *Nucl. Phys.* **B572** (2000) 243–265, [[hep-lat/9908041](#)].
- [35] M. Laine and O. Philipsen, *The non-perturbative QCD Debye mass from a Wilson line operator*, *Phys. Lett.* **B459** (1999) 259–264, [[hep-lat/9905004](#)].
- [36] K. Kajantie *et. al.*, *Non-perturbative Debye mass in finite T QCD*, *Phys. Rev. Lett.* **79** (1997) 3130–3133, [[hep-ph/9708207](#)].
- [37] E. Laermann and O. Philipsen, *Status of lattice QCD at finite temperature*, *Ann. Rev. Nucl. Part. Sci.* **53** (2003) 163–198, [[hep-ph/0303042](#)].
- [38] A. Karch and E. Katz, *Adding flavor to AdS/CFT*, *JHEP* **06** (2002) 043, [[hep-th/0205236](#)].

- [39] **QCD-TARO** Collaboration, I. Pushkina *et. al.*, *Properties of hadron screening masses at finite baryonic density*, *Phys. Lett.* **B609** (2005) 265–270, [[hep-lat/0410017](#)].
- [40] E. Laermann and P. Schmidt, *Meson screening masses at high temperature in quenched QCD with improved Wilson quarks*, *Eur. Phys. J.* **C20** (2001) 541–552, [[hep-lat/0103037](#)].
- [41] M. A. Vazquez-Mozo, *A note on supersymmetric Yang-Mills thermodynamics*, *Phys. Rev.* **D60** (1999) 106010, [[hep-th/9905030](#)].
- [42] C.-j. Kim and S.-J. Rey, *Thermodynamics of large- N super Yang-Mills theory and AdS/CFT correspondence*, *Nucl. Phys.* **B564** (2000) 430–440, [[hep-th/9905205](#)].
- [43] A. Kehagias and H. Partouche, *The exact quartic effective action for the type IIB superstring*, *Phys. Lett.* **B422** (1998) 109–116, [[hep-th/9710023](#)].
- [44] G. Policastro and D. Tsimpis, *R^4 , purified*, *Class. Quant. Grav.* **23** (2006) 4753–4780, [[hep-th/0603165](#)].
- [45] M. B. Green and C. Stahn, *D3-branes on the Coulomb branch and instantons*, *JHEP* **09** (2003) 052, [[hep-th/0308061](#)].
- [46] S. de Haro, A. Sinkovics, and K. Skenderis, *A supersymmetric completion of the R^4 term in IIB supergravity*, *Phys. Rev.* **D67** (2003) 084010, [[hep-th/0210080](#)].